Recent advances on spinel-based protective coatings for solid oxide cell metallic interconnects produced by electrophoretic deposition

Liquid Activated Carbon (LAC) – enhanced microwave remediation of PAH - contaminated soils

Pietro P. Falciglia*[a], Guido De Guidi[b,c], Fabiana Vento[b], Guglielmo Finocchiaro[b], Elisa Castro[a], Monica Granetto[d], Tiziana Tosco[d] and Federico G.A. Vagliasindi[a]

[a]*Dipartimento di Ingegneria Civile e Architettura, Università di Catania, Viale Andrea Doria 6, 95125, Catania, Italy*

[b]*Dipartimento di Scienze Chimiche, Università di Catania, Viale Andrea Doria 6, 95125, Catania, Italy*

[c]*Centro di ricerca per l'analisi, il monitoraggio e le metodologie di minimizzazione del rischio ambientale (CRAM3RA), Università di Catania, Italy*

[d]*Dipartimento di Ingegneria dell'Ambiente, del Territorio e delle Infrastrutture, Politecnico di Torino, corso Duca degli Abruzzi 24, 10129 Torino, Italy*

*Corresponding author. E-mail: pietro.falciglia@unict.it

Published in

Separation and Purification Technologies

Volume 331, 1 March 2024, 125628

https://doi.org/10.1016/j.seppur.2023.125628

Abstract

A new Liquid Activated Carbon (LAC)-enhanced micro-wave (MW) treatment was studied in the remediation of PAH-contaminated soils. The role of different doses of LAC was studied at the bench-scale varying MW input and irradiation times. Laboratory transport tests were also designed to assess the potential mobility of LAC suspensions in unsaturated porous media under the effect of gravity, thus simulating field application via ground flooding and gravity-driven percolation.

The main results revealed that the LAC can significantly increase the MW electric field absorbing performance of the irradiated medium, leading to very high soils temperatures up to ~1100 °C within 3-min irradiation time (LAC 10%). This resulted in largely shortened PAH removal kinetics. A LAC dose of 5% led to a total PAH removal in 5 min, whereas the maximum dose of 5% shorted this time to 2 min. Transport tests evidenced a good mobility of LAC when applied by gravity-driven percolation, without active injection. In 18 cm long columns, approximately 30% of LAC was retained, with a fairy homogeneous distribution along the bed length. Experimental and modelling results validate the concept of the LAC-enhanced MW heating and the fundamental role of the liquid enhancer for in situ remediation interventions.

Keywords: in situ soil remediation, thermal desorption, microwave enhancers, nano-remediation, colloidal activated carbon, Polycyclic Aromatic Hydrocarbons (PAHs).

1. Introduction

Polycyclic Aromatic Hydrocarbons (PAHs)-contaminated soil is a very important concern worldwide [1]. For instance, about 50% of the 1400 federal US-EPA contaminated sites are severely impacted by this class of contaminants [2]. PAHs are organic compounds mainly generated by pyrolysis or incomplete combustion of organic matter during anthropogenic (fossil fuel or coal tar industries, waste incineration) or natural activities (volcanic eruption, forest fire) [3]. PAHs are ubiquitous and very persistent in the environment with a strong affinity with soil particles. Their carcinogenic nature represents a threat to human health [4–6]. Then, the pathways of human exposure to PAHs make remedial activities strictly needed but very challenging, due to the contaminant nature and their strong interaction with soil particles. Various chemico-physical and biological technologies have been proposed so far for PAH-contaminated soils, however their poor biodegradability and low water solubility make most of these remediation alternatives inappropriate or ineffective [3]. In particular, biological-based treatments are still ineffective or long-clean-up time requiring. Moreover, biological PAH remediation is strongly affected by concentration of heavy metal in soil, with a reduction of bioactivity, dysfunction and retardation on microbial enzymatic and metabolic functions [7]. In any cases, high PAH concentrations represent a strong limit in remedial process [8]. As a consequence, rapid alternatives for effective decontamination interventions are needed. Particular interest has been recently shown in enhanced-thermal techniques [9].

Microwave (MW) heating has recently been showed as a potent technology in several environmental applications [10]. The key factor is the thermal process called dielectric heating. It is based on the passive ability of the irradiated matrices to immediately and largely convert the MW absorbed energy into heat. The heat production, expressed by Eq. 1 [11], results in a temperature increase able to trigger several contaminant removal mechanisms [12,13]. In dielectric heating, the heat ($\dot{Q}$) generated per unit of soil volume during the irradiation depends on the dielectric properties of the irradiated medium expressed by the dielectric loss factor (ε'') and electromagnetic field (E):

$$\dot{Q} = \frac{1}{2}\omega\epsilon_0\varepsilon''\left|E_{max}^2\right| = \omega\epsilon_0\varepsilon''\left|E^2\right| \quad (1)$$

where ω (MW angular frequency) = $2\pi f$ (with f being the MW frequency) [Hz], ε_0 is free space permittivity [-], E_{max} is maximum local electromagnetic field value [V/m], E is the effective local electromagnetic field value

[V/m].

Our recent study showed the ability of MW heating in removing selected PAHs from soils [14]. The results revealed removals of 70 to 100% with the highest values achievable only applying the maximum power investigated. This is correlated to the dielectric properties of the irradiated matrix: soil is considered transparent to MWs, and PAHs present a low-medium dielectric constant. Then, the treatment still results as potential energivorous, while low or moderate costs are strictly desired. In general, the literature studies demonstrate that MW heating is heavily limited when irradiated media have poor dielectric features [10]. However, they can be improved by adding specific MW catalysts (enhancers) to the contaminated soil. Several solid enhancers have been largely investigated so far in MW lab-scale applications: Cu_2O [15,16], NaOH [15,17], MnO_2 [17,18], graphite [15,16], ferrite ($MgFe_2O_4$) [19] or carbon nanotubes [20]. One of the most used is the activated carbon (AC) in the granular or powder forms, widely employed for a number of other environmental applications, e.g. water filters [16,21–24]. However, its granular nature requires the excavation of the matrix before the enhancer-soil mixing phase [25], thus limiting the enhanced-MW heating treatment only to the ex-situ applications. On the other hand, world environmental policies encourage the application of in situ technologies due to their lower risk and higher social sustainability [9], making the investigation of liquid MW-enhancer a very active research topic [26].

In the continuous search for liquid enhancing agents, Liquid Activated Carbon (LAC) is an innovative and non-hazardous material that could represent a very favourable alternative to granular forms. LAC is a highly concentrated water-based suspension consisting of nano-to-micron-scale activated carbon, typically applied in groundwater to form adsorptive/reactive zones for contaminant removal from the aqueous phase, and recently in particular for per- and polyfluoroalkyl substances (PFAS) remediation [27]. LAC conventional use includes low-pressure injection through wells or direct push injection, with the dual function of adsorbing contaminants onto AC particles and stimulating organic biodegradation [28,29]. LAC use in enhanced-MW treatments, still unexplored, would allow to combine the high dielectric properties of solid AC jointly with the potential application in in situ applications (without soil excavation). Literature and laboratory studies usually report a high LAC mobility in the porous medium, on average higher than other nano- or micro-materials typically applied for in-situ remediation. Niarchos et al. reported the breakthrough of 22% of the injected colloidal

activated carbon with a particles' size distribution between 1 and 2 μm in columns packed with a silty loam [30]. Surface and colloidal stabilization with oxidative pre-treatment or application of anionic stabilizer can further enhance activated carbon mobility with a breakthrough of up to 85% [31]. If an extremely high mobility can be potentially an issue when these materials are applied in groundwater, this characteristic represents a positive factor in view of their possible application in soils, opening perspectives for LAC delivery in top soils or at the bottom of excavated areas directly by ground flooding and percolation via gravity, similarly to liquid (non-viscous and particle-free) reactants used for other in situ soil treatments [32].

In the present work, a novel liquid activated carbon-enhanced MW treatment was investigated at the lab-scale to remediate PAH-contaminated soils. The influence of different experimental conditions (irradiation power, heating time, LAC dose) on soil temperature increase and PAH removal kinetics was investigated. LAC particles were characterized in terms of size, morphology and colloidal stability, assessing the impact of water chemistry on the potential aggregation, sedimentation and reduced mobility in the porous medium. Laboratory transport tests were designed to assess, at a preliminary level, the potential mobility of LAC suspensions in unsaturated porous media under the effect of gravity, studying their percolation in sand-packed partially-saturated columns and evaluating the final particle distribution in the porous medium. This is expected to show the potentiality of the investigated treatment in terms of clean-up time, decontamination effectiveness and environmental sustainability.

2. Materials and Methods

2.1 Liquid activated carbon characterization

A commercial LAC was used in all tests. The nominal composition included colloidal activated carbon (nominal size 1-2 μm, particle concentration 320 g/l) and di-hydrated calcium sulfate (nominal concentration < 10%). The suspension density (1.178±0.002 g/cm^3) was estimated via gravimetric method. After centrifugation, the density of the supernatant solution (1.013 g/cm^3) and, through a mass balance, the bulk particle density (1.55 g/cm^3) were determined. The distribution of the particle size and the surface charge were obtained using a Dynamic Light scattering (DLS, ZetaSizer Nano ZSP, Malvern, UK) for LAC suspensions diluted to 100 mg/l or 500 mg/l (corresponding to AC particle concentrations of 32 and 160 mg/l, respectively) in deionized water (DI) or in tap water (TW) (the latter to mimic field-like conditions). The tap water was collected from the municipal water supply network of Torino and analyzed for salts, pH, EC and TDS (Table

S2 in Supplementary Information). 5 replicates (each comprising 10 measurements) were run for each tested condition to ensure statistically reliable results.

Scanning Electron Microscopy (Inspect S, FEI Company, US) images were used to assess the LAC particle morphology. The SEM images were processed using the freeware software ImageJ (National Institutes of Health, US) to automatically identify the individual particles and, for each of them, to calculate particle area, perimeter, Feret diameter, and sphericity. Assuming a particle spherical shape, the diameter of each particle was then calculated as $D_{SEM} = 2A^{0.5}$, and the particle size distribution was compared with DLS results. A dried LAC sample was analyzed using XRD (SmartLab SE with D/teX Ultra 250 detector, Rigaku, JP) operated at 30 mA and 40 kV over a scan range from 5o to 90° (2θ) with a scan speed of 10.00°/min ad a step width of 0.01°. The colloidal stability of the LAC diluted in deionized water and in tap water to a concentration of 500 mg/l (160 mg/l of AC particles) was studied in sedimentation tests. To this aim, a set of 10 ml sacrificial vials was prepared for each studied solution. A sample of the supernatant was collected at fixed time (0.1, 2.5, 18, 24, 48 h) and analyzed for the particle concentration using UV-vis spectrophotometry (Specord S600, Analytic Jena, Germany; monitored wavelength 500 nm, calibration curves in Figure S2 in Supplementary Information) and for particle size using DLS.

2.2 LAC-enhanced MW treatments

A model soil (*Che.Mi.Fil., Italy*) (**Table 1**) was artificially contaminated with a PAH-dichloromethane (DCM) solution. Four PAHs [Fluorene (Flu), Phenanthrene (Phe), Anthracene (Ant) and Pyrene (Pyr) from the US-EPA priority list (*Sigma-Aldrich, Italy*) (Table S1 in Supplementary Information) was dissolved in the solvent, then mixed with the soil. The PAH-DCM-soil mixture was shacked for 1 hour using a *Büchi* rotavapor until the total DCM evaporation. The PAH-contaminated soil was stored sealed at 4 °C before initial contaminant concentration (C_0) analysis or MW heating simulated experiments. For the LAC-enhanced MW treatments, different doses (2.5 – 10.0%) of LAC were manually mixed with the soil before irradiation. SEM analysis of the LAC-soil system was also performed. MW and LAC-MW heating treatments were simulated using a custom-made bench-scale oven working with a 1-kW (f = 2.45 GHz) magnetron and a MW cavity volume of 31 l. The oven cavity was coupled with an exhaust gas line with a capture (condensing) section and a vacuum pump. For the experiments (conducted in triplicates), 15 g of PAH-contaminated soil samples (with or without LAC addition) were irradiated for a maximum time of 5 min (Power range = 440 – 1000 W). Soil temperature

(*T*) profiles were monitored using a 1.5 mm type-k thermocouple system. After the MW treatment, the soil samples were sealed and stored at 4 °C, then analyzed for PAH residual concentrations (C) and removal (R, %) calculations: $R = [(C_0 - C)/C_0]*100$. C values and re-condensed PAH or PAH-by-products (for soil samples contaminated with Anthracene) were quantified using HPLC analysis.

The experimental data (*C, t*) were least-squares fitted to an exponential decay curve [33]:

$$C = C_0 e^{-kt^n} \quad (2)$$

where *k* is the decay rate term (min^{-1}) and *n* is the shape term (-).

The desorption parameters and the correlation coefficient r^2 were obtained via least-squares fitting for all tests.

2.3 Extraction procedures and analytical methods

The PAHs present in the soil were recovered with dichloromethane (DCM) applying the EPA method 3540C. 1,2-dinitrobenzene was used as standard to verify the quantitative extraction [34]. Briefly, extraction was carried out in absence of light for 24h using a sub sample of 15 g and the correct amount of DCM (twice the volume of the used Soxhlet) as solvent. At the end of the extraction, the solvent was removed by means a rotavapor. The obtained sample was dissolved in acetonitrile in a warm (35 °C) bath for 10 min under ultrasonic field and filtered with a 0.2 μm PTFE filter syringe (*Millipore*). The extracted sample was dried under nitrogen and re-dissolved in a mixture of H_2O : ACN (70:30) before the HPLC analyses. The HPLC analyses of extracted compounds were performed with *Hewlett-Packard* 1100 equipped with on-line diode array detector (DAD), and a *Kontron* SFM fluorescence detector (FLD). A mixture water : acetonitrile (30:70 v/v) was used as mobile phase (flow 1mL/min) in isocratic mode for the extraction of Ant and its by-products using a reverse-phase C_{18} column (*Lichrosphere*; 4.6 mm x 250 mm). For PAHs mixture a gradient flow (1mL/min) was used to elute the compounds as follow increasing the % v/v of acetonitrile:

- 0-16 min from 75 to 85%,
- 16-27 min 85%,
- 27-55 min, from 85 to 90%,
- 55-60 min, back to 75%.

The chromatographic run was monitored at 265/389 ($\lambda_{exc/em}$) nm from 0 to 60 min (for Flu, Ant, Pyr, and Chr) [34].

2.4 Column transport experiments

The mobility of LAC in unsaturated porous media was investigated in column transport tests. Deionized water or tap water were used, depending on the test. A vertical plexiglass column (inner diameter 1.6 cm) was wet-packed with 60 g of silica sand (Dorsilit n. 8, Germany; 0.415 - 0.5 mm) to a length of 18 cm. Before packing, the sand was washed and sonicated in order to remove possible residual colloids, following the procedure described in [35], and degassed before packing to ensure the complete removal or residual air micro-bubbles from sand grain surface. Adjustable end fittings were used at both upper and lower ends, with polypropylene filters (mesh: 120 µm mesh) to prevent sand entering in the tubing without hindering LAC passage. The detailed protocol included:

- Pre-flushing in saturated conditions for at least 1 hour at a constant discharge rate of 0.75 ml/min using a peristaltic pump (Ismatec Reglo Analog MS-4/8, Germany).
- Tracer test (saturated conditions): injection of bromophenol blue solution at 0.75 ml/min for 50 minutes, followed by the injection of tracer-free solutions for additional 50 mins. The injected and effluent bromophenol blue concentrations were monitored in-line with a UV-vis spectrophotometer (Specord S600, Analytik Jena, Germany) equipped with flow-through cells with 5 mm lightpath at a wavelength of 595 nm. The tracer tests were interpreted using MNMs [36] to determine the saturated porosity and dispersivity coefficient and consequently the pore volume (**Table 3**).
- Column drainage: the column was further flushed for additional 5 pore volumes, then the flow was stopped and the outlet of the column was disconnected from the tubing leading to the flow-through cell, and let drain under gravity until no drops were recovered at the outflow for at least 5 mins.
- LAC infiltration (unsaturated conditions): the LAC transport was studied under gravity in the unsaturated medium to mimic a possible application at the field scale. To this aim, a suspension was prepared diluting 6 g of stock LAC (1.92 g of AC particles) in a volume of deionized (or tap) water equal to the pore volume, thus reaching a particle concentration of 113 g/l. The applied volume was chosen equal to the saturated pore volume to ensure that the suspension can potentially fill the pores of the system while flowing through it. The applied suspension was prepared to reach a 1:10 mass ratio of LAC suspension to soil mass (i.e. 6 g_{LAC}: 60 g_{soil}, corresponding to approximately 1 $g_{particle}$: 30 g_{soil}), which is in line with typical LAC doses adopted for field applications. The LAC suspension

was applied on top of the column and let drain through it under gravity. The effluent was collected at a frequency of 10 s. The volume of each sample was measured to determine the effluent discharge, and the samples were then analysed with UV-vis spectrophotometry to determine the LAC particle breakthrough curve.

At the end of the test, the column was extruded and dissected in 9 or 10 aliquots, depending on the test, each corresponding to a column length of approximately 2 cm, to determine the profile of retained LAC particles. Each sample was introduced in a known volume of deionized water and sonicated for 10 min to promote LAC detachment. The supernatant was then sampled, and the LAC concentration was measured with UV-vis spectrophotometry. The procedure was repeated three times on each sample to ensure complete recovery of the particles. After LAC extraction, the sand aliquots were dried and weighted and the retained concentration (mass of LAC particles per unit mass of sand) was calculated via a mass balance for each column aliquot, thus allowing the reconstruction of the concentration profile.

3. Results and discussion

3.1 LAC characterization

SEM images were acquired for the LAC suspensions at various dilutions. An example is reported in **Figure 1a**. The analysis evidenced a sharp-cornered morphology, without a predominant dimension. Most particles are in the nanometer range, with few larger ones in the order of 1-3 μm. Three SEM images were selected to extract the particle size distributions of the samples (see Figures S3 and S4 in the Supplementary Information for the individual images, particle size distributions and an example of the extraction procedure). **Figure 1b** shows the results in terms of number percent distribution. The distribution reports a main peak at approximately 170 nm, with a secondary peak around 550 nm, and a non-negligible number of particles close to or above 1 μm, thus indicating that most of them are in the nanometer range. From the cumulant distribution (not reported), D_{10}, D_{50} and D_{90} equal respectively to 148 nm, 292 nm and 1053 nm were obtained. The particle size measured using DLS indicated a Zeta-average value of 403.5±30.11 nm for particles dispersed in deionized water, and 454±53.78 nm for particles dispersed in tap water. The size distribution reported in terms of scattering intensity (Figure S5 in the Supplementary Information) also in this case evidenced a multi-modal shape, characterized by a main peak at 355.5±66.65 nm (for deionized water) or 401±141.0 nm (for tap water) and an associated shoulder peak at lower size (146.4±40.89 nm for deionized water, 178.2±53.76 nm

approximately), the latter not being clearly identifiable in all samples. In some samples, a (limited) peak in the range above 5000 nm appeared, in particular for the samples dispersed in tap water, suggesting the presence of a small number of particles (or, more likely, aggregates) in the micrometer range. In order to allow a direct comparison with SEM results, the DLS particles distributions (usually reported in terms of intensity) were transformed in number distributions: the mean distribution obtained for samples dispersed in deionized water at 32 mg/l (directly comparable with the SEM samples) is reported in **Figure 1b**. The two curves are in good agreement. Also the DLS PSD showed a main peak 164 nm, and a second peak at larger size (460 nm), but did not capture particles larger than 1μm. From the cumulant distribution (not reported), D_{10}, D_{50} and D_{90} equal respectively to 137 nm, 179 nm and 416 nm were obtained. The measured Zeta potential was -21.2±2.0 mV for the samples dispersed in deionized water and -18.7±0.6 mV for samples in tap water, thus confirming the possibility of a slightly lower colloidal stability for the latter samples, even though no visual differences in terms of aggregation nor sedimentation were observed over 24 h. The pattern from XRD analysis (dried LAC particles) (Figure S1 in the Supplementary Information) shows the distinctive shape of activated carbon. Moreover, the characteristic peaks of di-hydrated calcium sulphate can be clearly observed at $2\theta = 29.23°$, 31,60° and 44.17°. The peaks found at $2\theta = 26.48°$, 37.92°, 39.28°and 43.48° can be associated to the presence of silica, which is often reported to be found in activated carbon as a by-product of the pyrolysis process [37,38]. The peaks at higher 2θ are likely attributable to Ni impurities [39,40].

The diluted suspensions prepared for the laboratory tests did not show significant sedimentation on a short time frame. However, in view of a potential LAC application in the field, the colloidal stability was also assessed on a longer time frame with sedimentation tests, performed diluting the stock LAC suspension in deionized water and in tap water at a concentration of 160 mg/l (**Figure 2**). The results evidenced a comparable behavior for particles dispersed in deionized water and in tap water. After a few hours, the particle concentration in the supernatant declined significantly, reaching an almost stable particle concentration close to 50 mg/l (**Figure 2a**). Correspondingly, the average size, reported in terms of mean Z-average, declined after an initial spot increase and reached an almost stable value around 250 nm. Both observations suggest that, in undisturbed conditions, the coarse fraction of the suspensions undergoes sedimentation, and only the fine fraction remains in suspension. Even though this behavior has a limited impact on the laboratory tests, which are performed in a shorter term, it can be relevant for field-scale applications, and suggests that attention should

be paid in the preparation time and storage conditions of the diluted suspensions prior injection or gravity delivery in the subsurface.

3.2 LAC-Enhanced MW treatments

3.2.1 Soil temperature profiles

The soil temperature profiles (T vs t) are given in **Figure 3a**. For all the run, an increasing trend was observed due to the progressive rise in MW energy absorbed by the irradiated samples. The data clearly show the large difference in temperature variation among samples with or without LAC addition. In presence of LAC, a maximum T value in the 400 - ~1100 °C range was found within the power and irradiation time range investigated. The maximum temperature was achieved for the 440 – LAC 10 treatment after just 2 min. Reasonably, higher temperatures could even be obtained for longer periods, however this cannot be observed because when t was 3 min the destruction of the crucible occurred due to the excess of its maximum tolerable temperature. This is attributable to the increased dielectric properties of medium given by the presence of the LAC, which in turns sharply increase its capability in concerting the MW electric field into heat. Conversely, a maximum temperature lower than 100 °C was obtained in absence of LAC even when the highest power (1000 W) was put in place. It is also relevant to notice the extreme rapidity of the heating process caused by the LAC addition with heating rates observed up to 370 °C min^{-1}. The rapidity of the heating also influenced the shape of the T-t curve, that was found almost linear in all cases. The short irradiation time applied did not allow the temperature values to reach a plateau with reduction of the curve slope due to the occurrence of heat dissipation phenomena, generally observed when small solid samples are irradiated into the MW cavity for long times [41]. The obtained temperature profiles show the general excellent thermic performance of the investigated LAC-soil system. This plays a further and more important role when data are compared with those reachable by the use of other liquid enhancers [26]. Very good results were already found glycerol-enhanced MW treatments, but very farer from these. In general, the use of glycerol (dose 5%) allows a maximum temperature value of 334 °C by applying a more energivorous operating condition (P = 650 W; t = 10 min). Then the addition of LAC can balance the reduction in the energy requested, resulting in a much less energivorous decontamination process. Similar T profiles can in fact be obtained applying a general reduced power with a larges LAC dose (i.e.: 300 – LAC 7.5 VS 440 – LAC 5). A linear increase in temperature with the LAC dose was also found independently of the applied irradiation time (**Figure 3b**). This reflects the MW

heating theory expressed by Eq.1 for which the heating rate is proportionally direct to the dielectric features of the medium. Therefore, a linear increase in LAC dose contributes in a linear increase in the dielectric loss factor value. The observed trend will be also useful to predict the optimal LAC dose in view of a selected temperature target.

3.2.2 Contaminant removal, mechanisms, and modelling

PAH removal (*R*) curves calculated from residual contaminant concentration as function of the LAC dose applied for 1, 2 and 3 min irradiation (*t*) and a power of 440 W are given in **Figure 4**. They clearly show that the capacity of the treatment in removing contaminants depends on the presence/absence the LAC and its dose and, consequently, on the temperature reached by the LAC-soil system. For instance, the temperatures of 153, 343 and 557 °C were recorded when the applied irradiation time was 1, 2 and 3 min (LAC dose 5%), respectively, allowing a progressive increase in single PAH removal up to ~96%. Higher LAC doses lead to the almost total removal due to temperatures values up to ~1100 °C. This demonstrated that the temperature effect and the relation between the treatment temperature and contaminant vaporization temperature (in the 298 – 448 °C range) are the main factor controlling the organic removal process. The highest PAH removals were found for the compounds having lower molecular weight (thus lower boiling points), consequently requiring minor heat of vaporisation. LAC colloidal particles resulted adsorbed on the soil surface with a distribution that depends on the LAC dose (**Figure 5**). LAC particles act as "hot spots", which transform the MW electric field energy into a large a rapid local temperature increase up to values even much higher than those recordable by the measurement system [20]. This leads to the destruction of the organic – soil grain force, resulting in thermal desorption processes with the consequent generation of volatile organic compounds (VOCs) [14]. The presence of moisture and the liquid phase of LAC contribute to the activation of contaminant vaporization processes [42]. This is further supported by the lowest PAH removals (<15%) found for the un-enhanced treatments for which temperatures lower than 100 °C were recorded. Despite the obtained data support the main criterion based on the PAH molecular structure and weight (vaporization temperature), the highest removals achieved for the chrysene (Chr) that presents the highest boiling point, suggesting that even contaminant selective heating takes place as co-removal mechanism. Chr has the highest polarity (log P) among the investigated compounds that contributes to a larger ability of the PAH to locally increase its

temperature. In fact, soil grain and PAHs can be heated at different rates, depending on their different dielectric ability [10].

Kinetic curves with residual concentration points and parameters from best fitting problem solving are given in **Figure 6** and **Table 2**, respectively. Data show a decrease in PAH-concentration with irradiation time with a rapidity depending on the conditions investigated (type of contaminant, power and LAC dose). Specifically, the effect of the LAC dose increase is clearly visible for the kinetics found for the treatments 440 – LAC 5, 440 – LAC 7.5, 440 and LAC 10 (**Figures 6c**, **6d**, **6e**, respectively) for which the time required for the total removal of the PAH compounds sharply tends to a significant reduction up to 2 min. The observed curves shape is that typical for conventional thermal desorption [33] or un-enhanced microwave heating [43] suggesting that LAC dose influence the heating rate of the process but does not change its nature. Curves show a trend that is typical for thermal removal of organics from porous media [33]. It includes two phases in sequence: the first describes the fast evaporating of the contaminant from the media caused by the synergic effect of various co-removal mechanisms (thermal desorption, water stripping, selective heating); the second expresses a limitation in contaminant removal rate due to the activation of internal diffusion phenomena. The calculated r^2 values in the 0.968 - 0.999 range (**Table 2**) demonstrated an excellent exponential fit of Eq. 2 with the experimental points. The effects of the treatments and the nature of the PAH-compound are clearly visible from k vs LAC dose plot depicted in **Figure 7**. K increase linearly with the LAC dose with the highest values observed for the contaminant with the highest polarity, suggesting that the activation energy needed for the PAH removal strictly depends on the PAH polarity. K values up to 3.417 min^{-1} highlight the thermic performance of the LAC-MW system especially in comparison with previous work on conventional or MW thermal desorption, reporting k values lower than 2 min^{-1}. MW heating of PAH-contaminated soils in absence of LAC is characterized by *k* values lower than 1 min^{-1} [14].

Residual PAH concentrations obtained by the application of the LAC-enhanced treatment allow the achievement of severe regulatory limits such the Italian ones. For instances, the maximum admissible residual concentration (Contamination Threshold Concentration – Concentrazione Soglia di Contaminazione, CSC - Law Decree 152/2006) for total PAHs of 10 mg kg^{-1} can be met in just 5 min also when the minimal power was applied (270 – LAC 10) (**Figure 6f**). Shorter times of 4.4 or 4.2 min can be enough for higher power and

a reduced LAC dose (300 – LAC 7.5 or 440 LAC, respectively). The shortest time of 1.4 min is achievable when the maximum power and dose are applied.

From literature [2], it is clear that available PAH-contaminated soil clean-up approaches cannot lead to a similar rapid and total decontamination result, especially considering bio- or phytoremediation alternatives. These and other chemico-physical techniques still show limited PAH removals and/or much longer required decontamination times.

3.2.3 By-product production and possible Ant degradation mechanisms

To shed light on the role of LAC, a possible pathway of Ant, among the different studied PAHs was investigated. Without LAC, only a minor percentage, less than 10% (**Figure 6**) of the residual Ant, as well as traces of by-products were recovered after the treatment. This phenomenon is due to the low temperatures (under 100 °C) of the soil in absence of LAC. On the other hand, the presence of LAC increases the temperature reached by the soil and this effect converts into a greater presence of by-products in the condensate. Investigating for example the fate of the Ant, the HPLC analysis reported in Figure 8a, shows Ant oxidized derivatives: 9,10-anthraquinone (1), 9-anthrone (2) eluting before Ant at a retention time of ~ 6 min, 9-hydroxyanthracene (3), and 9,10-dihydroxyanthracene (4), both eluting before Anthracene (Ant) at t_R of 3 and 7 min, respectively [34]. Oxidative reactions occur frequently in position sites 9 and 10 for Ant, because these are the most reactive sites. From these results a possible pathway of Ant was reported in Figure 8b [44]. By-products traces in the condensate suggest their formation during MW thermal remediation process. Furthermore, molecular bond breaking can modify the hallmark of light gases (CO_2, CO, H_2) that are generated during the stripping phase [45].

3.3 Column transport experiments

The mobility of the LAC suspensions under gravity effect was studied in the column transport tests in an unsaturated porous medium, to preliminarily verify whether this type of particle delivery could be potentially applied in the field. The LAC dispersion was applied on top of the partially saturated columns and let drain through it under gravity effect, with no pumping. The experimental results are in agreement with the good short-term colloidal stability observed for the LAC particles. The drained discharge, as intuition would suggest, was maximum at the beginning of the tests, and declined over time due to the dissipation of the applied head (Figure S6 in the Supplementary Information). For both tests the drainage stopped after 260 seconds from start.

The breakthrough curves (**Figure 9a**) show that the LAC suspension appeared at the column outlet approximately 1 minute after its application, and a concentration equal to the applied one was obtained at the column outflow 2.5 minutes after the beginning of the drainage test. A very similar behavior was observed for particles dispersed in deionized and tap water. To better quantify the particle retention in the column, the breakthrough curves and the recovered discharge curves have been processed to report the cumulated mass collected over time at the column outflow (**Figure 9b**). A minor discrepancy is observed between deionized and tap water, with the latter showing a slightly higher recovery. For both tests, the steepness of the curve decreases after reaching the breakthrough concentration plateau, due to the progressive decline in the drained discharge. The final recovered mass is in the 65-70% range, coherently with the good mobility expected for AC in the porous medium. The AC particles retained at the end of the test are quite homogeneously distributed along the columns (**Figure 9c**): the vertical concentration profile shows variations in the upper part of the column, while at larger depths an almost constant concentration is observed, with a slightly increasing trend from top to bottom. The almost constant profiles, along with $C/C_0 = 1$ reached by the breakthrough curves at the column outlet, indicate that particle retention is not controlled by mechanical filtration or ripening, which, would give rise to exponential or hyper-exponential profiles. Rather, blocking (i.e. limited to a maximum retainable concentration, in this case in the order of 10 mg/g) seems to be the controlling phenomenon, even though this hypothesis must be confirmed with additional tests and via numerical modeling of the experimental results.

4. Conclusions

The addition of liquid activated carbon (LAC) in soil largely increase the capacity of the irradiated media in MW electric field absorbing and, consequently, in converting within a very short time even a relatively low energy input into a very large temperature increase. The increase in LAC dose allows a progressive decrease in the energy required by the system in view of the complete removal of the PAHs from the soil. A maximum temperature of ~1100 °C within 3-min irradiation time was recorded when the maximum dose (10%) of LAC was used at the power of 440 W. On the other hand, even higher powers in unenhanced treatments led to temperatures lower 100 °C. The increased temperatures allow the faster shortening of the contaminant removal kinetics. Specifically, a LAC dose of 5% results in a total PAH removal in 5 min, whereas the removals lower than 15% are possible in un-enhanced MW. The findings reveal that PAH removal is mainly governed by

thermal desorption process. Contaminant striping, selective heating, and molecular bound breaking ere also demonstrated to have a key role.

The exponential model adopted in the PAH-removal kinetic study showed an excellent fit with PAH residual concentrations from experiment phase, with r^2 higher than 0.968. Kinetics parameters can be essential for further energy-cost analyses and scaling-up experiments towards LAC-enhanced MW heating real scale applicability.

The good LAC mobility observed in column transport tests opens optimistic perspectives for an effective delivery via gravity of the LAC suspensions, at least in permeable soils. This approach is typically not suitable for the emplacement of colloidal reactants in the unsaturated zone, due to their usual limited mobility in the porous medium compared to LAC. Further studies are undoubtedly needed at the next stage to elucidate the impact of soil grain distribution and applied LAC concentration to control deposited concentration, depth and uniformity of particles distribution within the treatment area.

A comparing with existing literature highlights that available chemico-physical or biological PAH-clean-up approaches cannot lead to a similar rapid and total decontamination result, still showing limited PAH removals and/or much longer required decontamination times.

Acknowledgments

This study was partially funded by the University of Catania within the “Piano di incentivi per la Ricerca di Ateneo 2020/2022” of the Department of Civil Engineering and Architecture, Project “Trattamenti Innovativi a MIcroonde per il Risanamento in situ di siti contaminati da composti Organici Xenobiotici (TIMIROX)”.

The authors wish to thank Prof. Paola Marini and Eng. Oliviero Baietto (Politecnico di Torino) for the support with SEM and XRD measurements and the Prof. Graziella Malandrino (Università di Catania) for the support with SEM measurements.

References

[1] C. Dai, Y. Han, Y. Duan, X. Lai, R. Fu, S. Liu, K.H. Leong, Y. Tu, L. Zhou, Review on the contamination and remediation of polycyclic aromatic hydrocarbons (PAHs) in coastal soil and sediments, Environ Res. 205 (2022) 112423. https://doi.org/10.1016/j.envres.2021.112423.

[2] S. Kuppusamy, P. Thavamani, K. Venkateswarlu, Y.B. Lee, R. Naidu, M. Megharaj, Remediation approaches for polycyclic aromatic hydrocarbons (PAHs) contaminated soils:

Technological constraints, emerging trends and future directions, Chemosphere. 168 (2017) 944–968. https://doi.org/10.1016/j.chemosphere.2016.10.115.
[3] Y. Abbas, W. Lu, H. Dai, X. Fu, R. Ye, H. Wang, Remediation of polycyclic aromatic hydrocarbons (PAHs) contaminated soil with double dielectric barrier discharge plasma technology: Influencing parameters, Chemical Engineering Journal. 394 (2020) 124858. https://doi.org/10.1016/j.cej.2020.124858.
[4] P.P. Falciglia, A. Catalfo, G. Finocchiaro, F.G.A. Vagliasindi, S. Romano, G. De Guidi, Microwave heating coupled with UV-A irradiation for PAH removal from highly contaminated marine sediments and subsequent photo-degradation of the generated vaporized organic compounds, Chemical Engineering Journal. 334 (2018) 172–183. https://doi.org/10.1016/j.cej.2017.10.041.
[5] S. Shukla, R. Khan, P. Bhattacharya, S. Devanesan, M.S. AlSalhi, Concentration, source apportionment and potential carcinogenic risks of polycyclic aromatic hydrocarbons (PAHs) in roadside soils, Chemosphere. 292 (2022) 133413. https://doi.org/10.1016/j.chemosphere.2021.133413.
[6] M.A. Mallah, L. Changxing, M.A. Mallah, S. Noreen, Y. Liu, M. Saeed, H. Xi, B. Ahmed, F. Feng, A.A. Mirjat, W. Wang, A. Jabar, M. Naveed, J.H. Li, Q. Zhang, Polycyclic aromatic hydrocarbon and its effects on human health: An overeview, Chemosphere. 296 (2022). https://doi.org/10.1016/j.chemosphere.2022.133948.
[7] M. Ali, X. Song, D. Ding, Q. Wang, Z. Zhang, Z. Tang, Bioremediation of PAHs and heavy metals co-contaminated soils: Challenges and enhancement strategies, Environmental Pollution. 295 (2022) 118686. https://doi.org/10.1016/j.envpol.2021.118686.
[8] M. Kumar, N.S. Bolan, S.A. Hoang, A.D. Sawarkar, T. Jasemizad, B. Gao, S. Keerthanan, L.P. Padhye, L. Singh, S. Kumar, M. Vithanage, Y. Li, M. Zhang, M.B. Kirkham, A. Vinu, J. Rinklebe, Remediation of soils and sediments polluted with polycyclic aromatic hydrocarbons: To immobilize, mobilize, or degrade?, J Hazard Mater. 420 (2021) 126534. https://doi.org/10.1016/j.jhazmat.2021.126534.
[9] Z. Han, S. Li, Y. Yue, Y. Tian, S. Wang, Z. Qin, L. Ji, D. Han, W. Jiao, Enhancing remediation of PAH-contaminated soil through coupling electrical resistance heating using Na2S2O8, Environ Res. 198 (2021) 110457. https://doi.org/10.1016/J.ENVRES.2020.110457.
[10] P.P. Falciglia, P. Roccaro, L. Bonanno, G. De Guidi, F.G.A. Vagliasindi, S. Romano, A review on the microwave heating as a sustainable technique for environmental remediation/detoxification applications, Renewable and Sustainable Energy Reviews. 95 (2018) 147–170. https://doi.org/10.1016/J.RSER.2018.07.031.
[11] P.P. Falciglia, P. Scandura, F.G.A. Vagliasindi, Modelling of in situ microwave heating of hydrocarbon-polluted soils: Influence of soil properties and operating conditions on electric field variation and temperature profiles, J Geochem Explor. 174 (2017) 91–99. https://doi.org/10.1016/j.gexplo.2016.06.005.
[12] A.J. Buttress, E. Binner, C. Yi, P. Palade, J.P. Robinson, S.W. Kingman, Development and evaluation of a continuous microwave processing system for hydrocarbon removal from solids, Chemical Engineering Journal. 283 (2016) 215–222. https://doi.org/10.1016/j.cej.2015.07.030.
[13] V.K. Tyagi, S.L. Lo, Microwave irradiation: A sustainable way for sludge treatment and resource recovery, Renewable and Sustainable Energy Reviews. 18 (2013) 288–305. https://doi.org/10.1016/j.rser.2012.10.032.
[14] P.P. Falciglia, G. De Guidi, A. Catalfo, F.G.A. Vagliasindi, Remediation of soils contaminated with PAHs and nitro-PAHs using microwave irradiation, Chemical Engineering Journal. 296 (2016) 162–172. https://doi.org/10.1016/j.cej.2016.03.099.

[15] R.A. Abramovitch, B.Z. Huang, M. Davis, L. Peters, Decomposition of PCBs and other polychlorinated aromatics in soil using microwave energy, Chemosphere. 37 (1998) 1427–1436. https://doi.org/10.1016/S0045-6535(98)00133-7.
[16] D. LI, Y. ZHANG, X. QUAN, Y. ZHAO, Microwave thermal remediation of crude oil contaminated soil enhanced by carbon fiber, Journal of Environmental Sciences. 21 (2009) 1290–1295. https://doi.org/10.1016/S1001-0742(08)62417-1.
[17] S. Yuan, M. Tian, X. Lu, Microwave remediation of soil contaminated with hexachlorobenzene, J Hazard Mater. 137 (2006) 878–885. https://doi.org/10.1016/j.jhazmat.2006.03.005.
[18] G. yi Huang, L. Zhao, Y. hua Dong, Q. Zhang, Remediation of soils contaminated with polychlorinated biphenyls by microwave-irradiated manganese dioxide, J Hazard Mater. 186 (2011) 128–132. https://doi.org/10.1016/j.jhazmat.2010.10.092.
[19] J. Chen, D. Zhong, H. Hou, C. Li, J. Yang, H. Zhou, L. Hu, L. Wang, Ferrite as an effective catalyst for HCB removal in soil : Characterization and catalytic performance, 294 (2016) 246–253. https://doi.org/10.1016/j.cej.2016.02.020.
[20] J. Chen, S. Xue, Y. Song, M. Shen, Z. Zhang, T. Yuan, F. Tian, D.D. Dionysiou, Microwave-induced carbon nanotubes catalytic degradation of organic pollutants in aqueous solution, J Hazard Mater. 310 (2016) 226–234. https://doi.org/10.1016/j.jhazmat.2016.02.049.
[21] L. Lin, S. Yuan, J. Chen, L. Wang, J. Wan, X. Lu, Treatment of chloramphenicol-contaminated soil by microwave radiation, Chemosphere. 78 (2010) 66–71. https://doi.org/10.1016/j.chemosphere.2009.09.054.
[22] X. Liu, X. Quan, L. Bo, S. Chen, Y. Zhao, M. Chang, Temperature measurement of GAC and decomposition of PCP loaded on GAC and GAC-supported copper catalyst in microwave irradiation, Appl Catal A Gen. 264 (2004) 53–58. https://doi.org/10.1016/j.apcata.2003.12.026.
[23] H.S. Tai, C.J.G. Jou, Immobilization of chromium-contaminated soil by means of microwave energy, J Hazard Mater. 65 (1999) 267–275. https://doi.org/10.1016/S0304-3894(98)00274-X.
[24] X. Liu, G. Yu, Combined effect of microwave and activated carbon on the remediation of polychlorinated biphenyl-contaminated soil, Chemosphere. 63 (2006) 228–235. https://doi.org/10.1016/j.chemosphere.2005.08.030.
[25] G. Wei, H. Liu, R. Zhang, Y. Zhu, X. Xu, D. Zang, Application of microwave energy in the destruction of dioxins in the froth product after flotation of hospital solid waste incinerator fly ash, J Hazard Mater. 325 (2017) 230–238. https://doi.org/10.1016/j.jhazmat.2016.11.078.
[26] P.P. Falciglia, G. De Guidi, A. Catalfo, G. Finocchiaro, M. Farina, M. Liali, G. Lorenzano, G. Valastro, F.G.A. Vagliasindi, Glycerol-enhanced microwave heating for ultra-rapid effective remediation of marine sediments highly contaminated with hydrocarbons, Sep Purif Technol. 189 (2017) 11–19. https://doi.org/10.1016/J.SEPPUR.2017.07.066.
[27] G. Niarchos, L. Ahrens, D.B. Kleja, G. Leonard, J. Forde, J. Bergman, E. Ribeli, M. Schütz, F. Fagerlund, In-situ application of colloidal activated carbon for PFAS-contaminated soil and groundwater: A Swedish case study, Remediation. (2023) 101–110. https://doi.org/10.1002/rem.21746.
[28] R. McGregor, Six pilot-scale studies evaluating the in situ treatment of PFAS in groundwater, Remediation Journal. 30 (2020) 39–50. https://doi.org/10.1002/REM.21653.
[29] R. McGregor, In Situ treatment of PFAS-impacted groundwater using colloidal activated Carbon, Remediation Journal. 28 (2018) 33–41. https://doi.org/10.1002/REM.21558.
[30] G. Niarchos, L. Ahrens, D.B. Kleja, F. Fagerlund, Per- and polyfluoroalkyl substance (PFAS) retention by colloidal activated carbon (CAC) using dynamic column experiments, Environmental Pollution. 308 (2022) 119667. https://doi.org/10.1016/j.envpol.2022.119667.
[31] A. Georgi, A. Schierz, K. Mackenzie, F.D. Kopinke, Colloidal activated carbon for in-situ groundwater remediation - Transport characteristics and adsorption of organic compounds in

water-saturated sediment columns, J Contam Hydrol. 179 (2015) 76–88. https://doi.org/10.1016/j.jconhyd.2015.05.002.
[32] G.M. Wilton, J.I. Gerhard, D.W. Major, Carbon injection to support in-situ smoldering remediation, Remediation. 33 (2022) 39–51. https://doi.org/10.1002/rem.21737.
[33] P.P. Falciglia, M.G. Giustra, F.G.A. Vagliasindi, Low-temperature thermal desorption of diesel polluted soil: Influence of temperature and soil texture on contaminant removal kinetics, J Hazard Mater. 185 (2011) 392–400. https://doi.org/10.1016/j.jhazmat.2010.09.046.
[34] G. de Guidi, V. Librando, Z. Minniti, E. Bolzacchini, G. Perrini, G. Bracchitta, A. Alparone, A. Catalfo, The PAH and Nitro-PAH Concentration Profiles in Size-Segregated Urban Particulate Matter and Soil in Traffic-Related Sites in Catania, Italy, Polycycl Aromat Compd. 32 (2012) 439–456. https://doi.org/10.1080/10406638.2011.654306.
[35] F. Mondino, A. Piscitello, C. Bianco, A. Gallo, A. de Folly D'Auris, T. Tosco, M. Tagliabue, R. Sethi, Injection of Zerovalent Iron Gels for Aquifer Nanoremediation: Lab Experiments and Modeling, Water 2020, Vol. 12, Page 826. 12 (2020) 826. https://doi.org/10.3390/W12030826.
[36] C. Bianco, T. Tosco, R. Sethi, A 3-dimensional micro- and nanoparticle transport and filtration model (MNM3D) applied to the migration of carbon-based nanomaterials in porous media, J Contam Hydrol. 193 (2016) 10–20. https://doi.org/10.1016/J.JCONHYD.2016.08.006.
[37] M. Wu, P. Li, Y. Li, J. Liu, Y. Wang, Enteromorpha based porous carbons activated by zinc chloride for supercapacitors with high capacity retention, RSC Adv. 5 (2015) 16575–16581. https://doi.org/10.1039/C4RA13428A.
[38] P. Dutournié, M. Bruneau, J. Brendlé, L. Limousy, S. Pluchon, Mass transfer modelling in clay-based material: Estimation of apparent diffusivity of a molecule of interest, Comptes Rendus Chimie. 22 (2019) 250–257. https://doi.org/10.1016/J.CRCI.2018.10.008.
[39] A.I. Bakti, P.L. Gareso, Characterization of Active Carbon Prepared from Coconuts Shells using FTIR, XRD and SEM Techniques, Jurnal Ilmiah Pendidikan Fisika Al-Biruni. 7 (2018) 33–39. https://doi.org/10.24042/JIPFALBIRUNI.V7I1.2459.
[40] N. Sofyan, P. Sekaringtyas, A. Zulfia, A. Subhan, Use of carbon pyrolyzed from rice husk in LiFePO4/V/C composite and its performance for lithium ion battery cathode, IOP Conf Ser Earth Environ Sci. 105 (2018) 012023. https://doi.org/10.1088/1755-1315/105/1/012023.
[41] P.P. Falciglia, C. Ingrao, G. De Guidi, A. Catalfo, G. Finocchiaro, M. Farina, M. Liali, G. Lorenzano, G. Valastro, F.G.A. Vagliasindi, Environmental Life Cycle Assessment of marine sediment decontamination by citric acid enhanced-microwave heating, Science of The Total Environment. 619–620 (2018) 72–82. https://doi.org/10.1016/J.SCITOTENV.2017.11.085.
[42] O. Ogunniran, E.R. Binner, A.H. Sklavounos, J.P. Robinson, Enhancing evaporative mass transfer and steam stripping using microwave heating, Chem Eng Sci. 165 (2017) 147–153. https://doi.org/10.1016/J.CES.2017.03.003.
[43] P.P. Falciglia, F.G.A. Vagliasindi, Remediation of hydrocarbon polluted soils using 2.45 GHz frequency-heating: Influence of operating power and soil texture on soil temperature profiles and contaminant removal kinetics, J Geochem Explor. 151 (2015) 66–73. https://doi.org/10.1016/J.GEXPLO.2015.01.007.
[44] V. Librando, G. Bracchitta, G. de Guidi, Z. Minniti, G. Perrini, A. Catalfo, Photodegradation of Anthracene and Benzo[a]anthracene in Polar and Apolar Media: New Pathways of Photodegradation, Polycycl Aromat Compd. 34 (2014) 263–279. https://doi.org/10.1080/10406638.2014.892887.
[45] V. Risoul, H. Richter, A.L. Lafleur, E.F. Plummer, P. Gilot, J.B. Howard, W.A. Peters, Effects of temperature and soil components on emissions from pyrolysis of pyrene-

contaminated soil, J Hazard Mater. 126 (2005) 128–140.
https://doi.org/10.1016/J.JHAZMAT.2005.06.019.

Figures

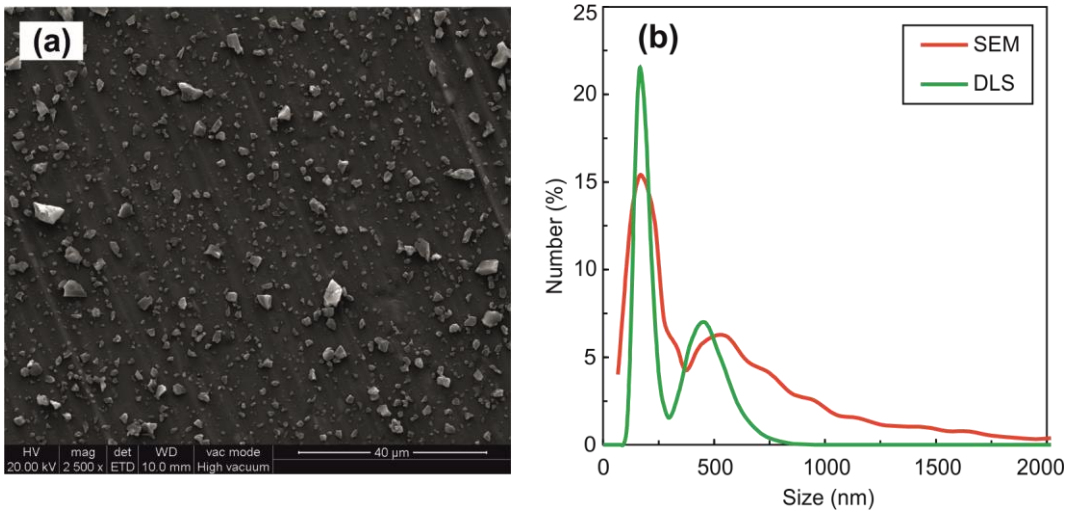

Figure 1. SEM image of LAC suspension diluted to 32 mg/l in deionized water (the drop was deposited on the sample holder and allowed drying at ambient conditions) **(a)** and number particle size distribution obtained from the analysis of SEM images (red curve) and from DLS measurements (green curve) **(b)**.

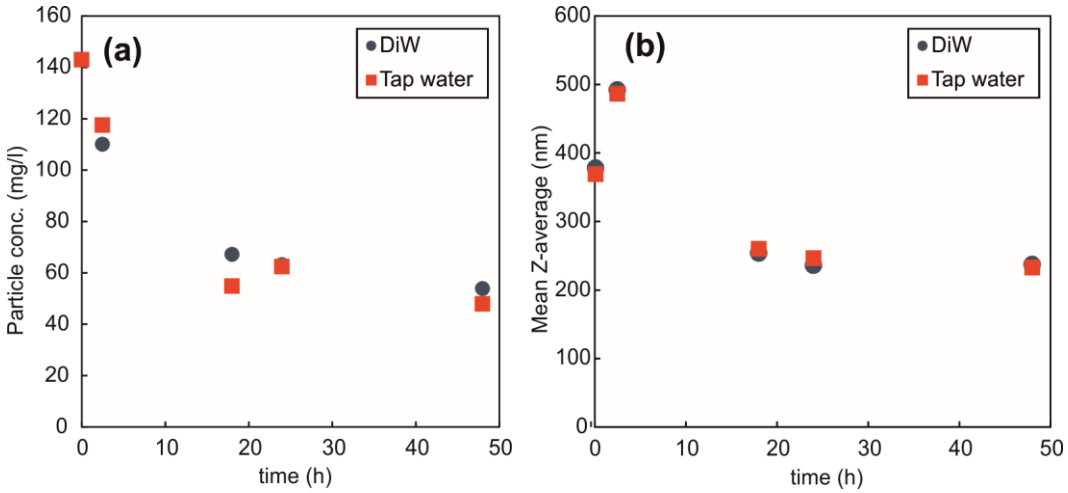

Figure 2. Particle concentration **(a)** and mean zeta-average **(b)** over time for LAC samples diluted in deionized water (DiW, blue circles) and tap water (red squares) at 160 mg/l.

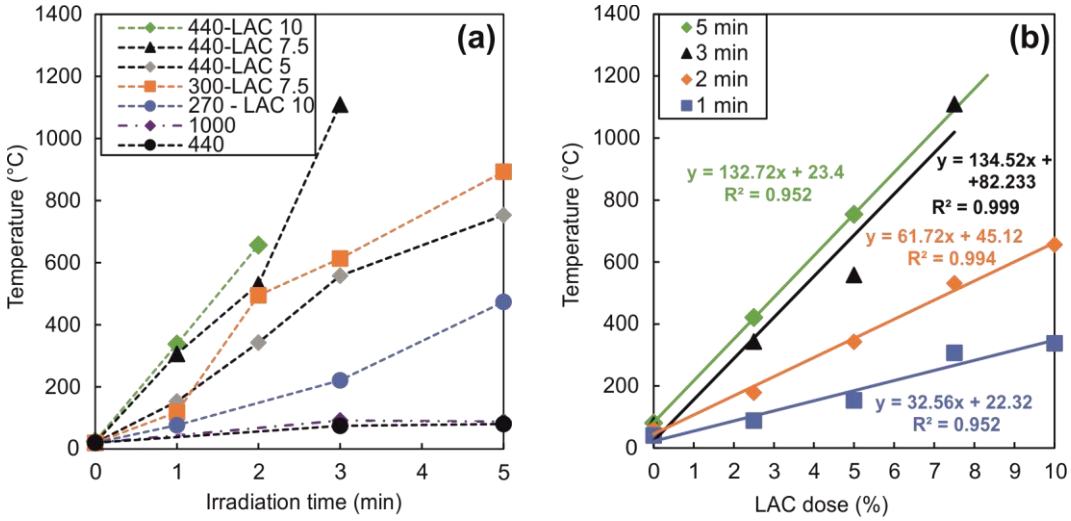

Figure 3. Soil temperature (*T*) profiles during MW irradiation for all the tests **(a)** and as a function of the LAC dose (%) **(b)**.

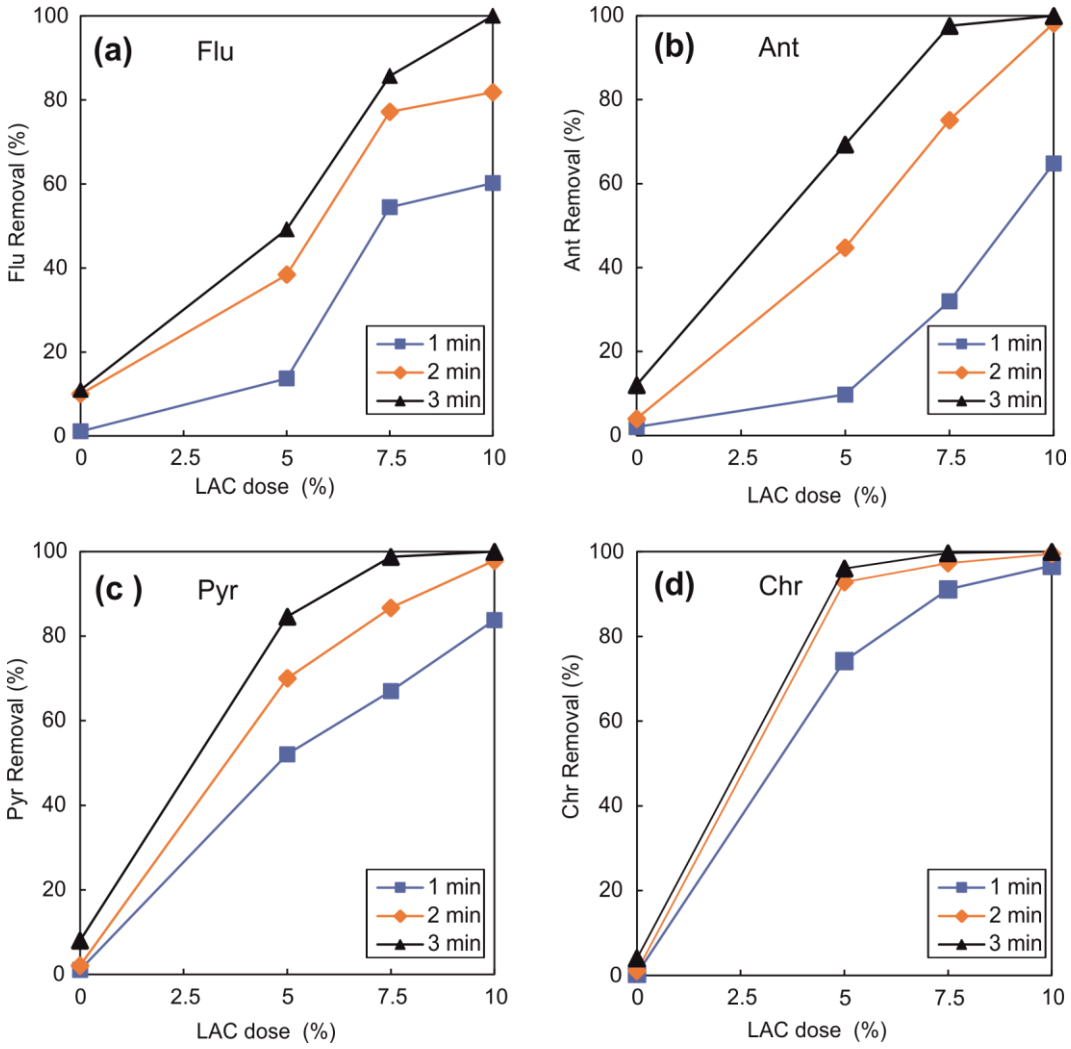

Figure 4. Single PAH-removal (%) as a function of the LAC dose added for 1, 2 and 3-min irradiation times (applied power 440 W).

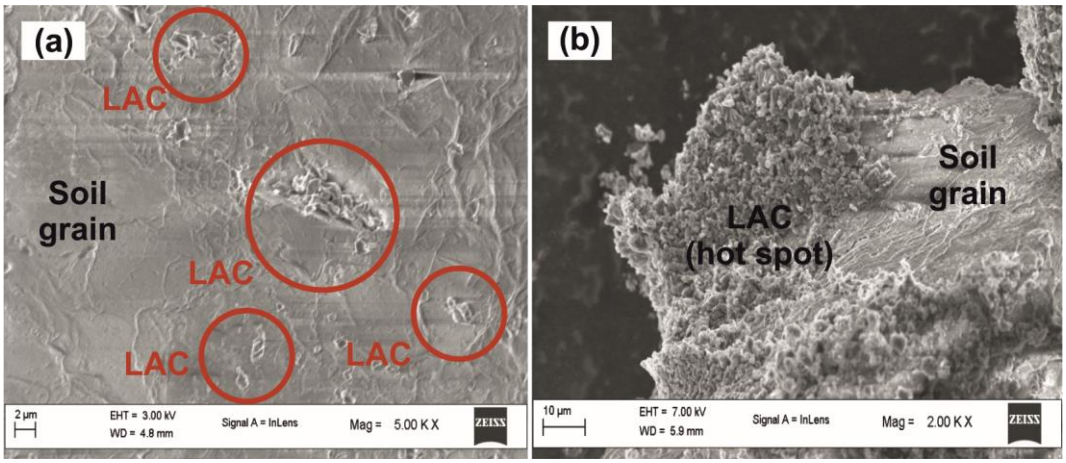

Figure 5. SEM images of LAC-soil mixture before irradiation with small (LAC dose 5%) **(a)** and large (LAC dose 10%) **(b)** LAC aggregates.

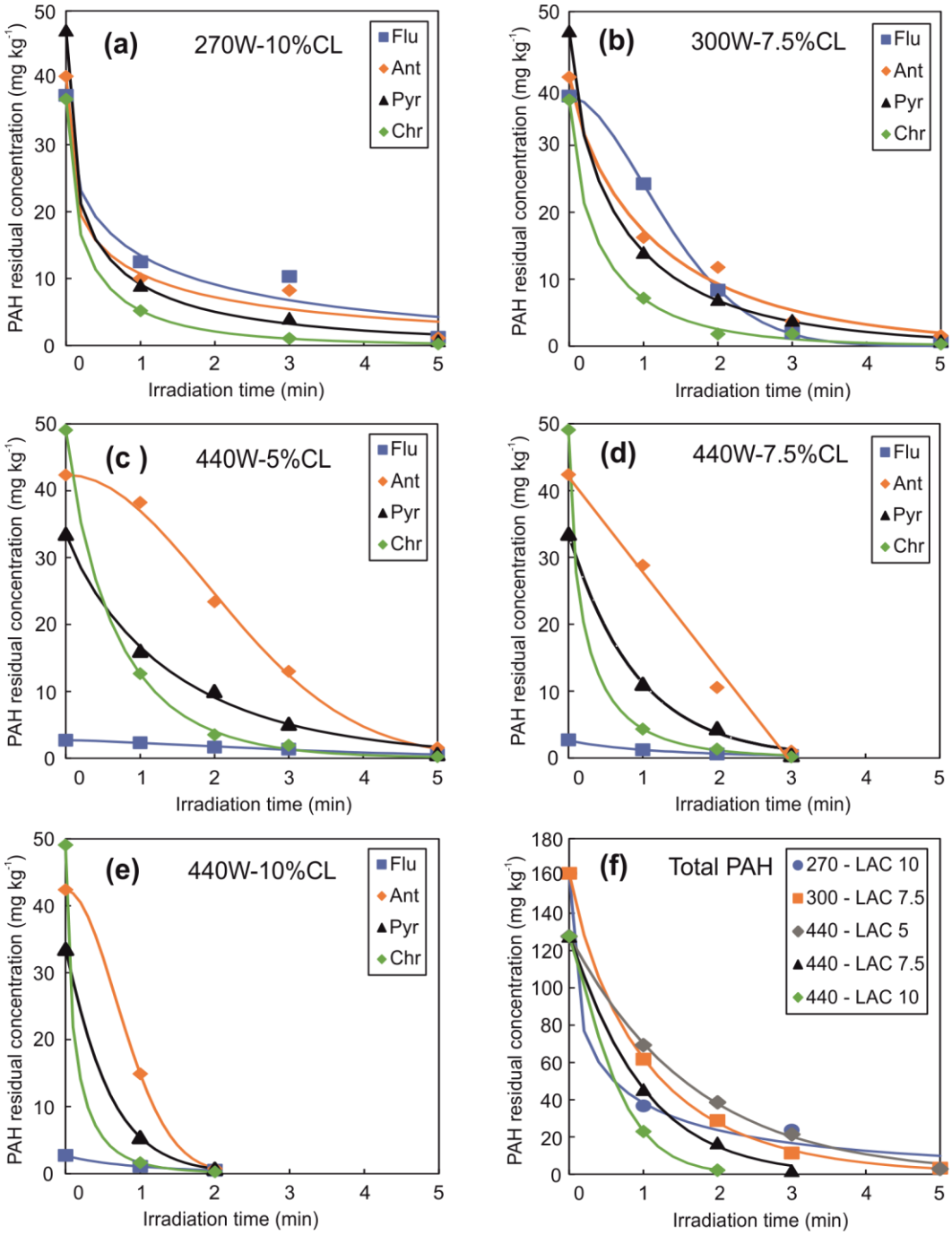

Figure 6. Single PAH residual concentration with irradiation time and model curves for the investigated treatments: 270 - LAC 10 **(a)**, 300 - LAC 7.5 **(b)**, 400 - LAC 5 **(c)**, 400 - LAC 7.5 **(d)** and 400 - LAC 10 **(e)**. Total PAH residual concentration with irradiation time and related best fitting model curves **(f)**.

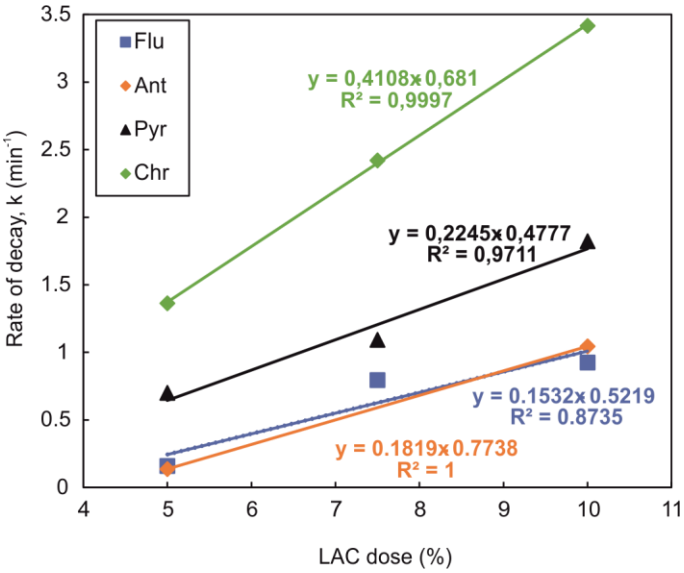

Figure 7. Rate of decay (k) as a function of the LAC dose (%) for the single PAH investigated (applied power 440 W).

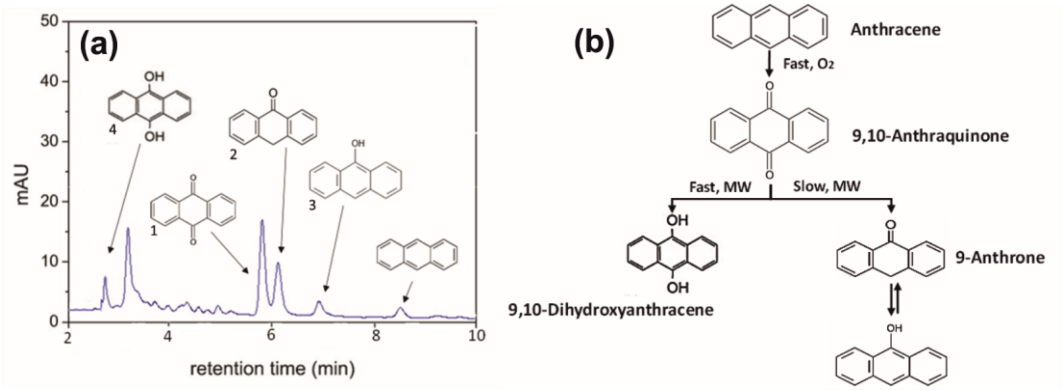

Figure 8. HPLC trace of Ant obtained in presence of LAC. (1) 9,10-anthraquinone, (2) 9-anthrone, (3) 9-hydroxyanthracene, (4) 9,10-dihydroxyanthracene **(a)**. Possible mechanism of Ant degradation exposed to microwave in presence of LAC **(b)**.

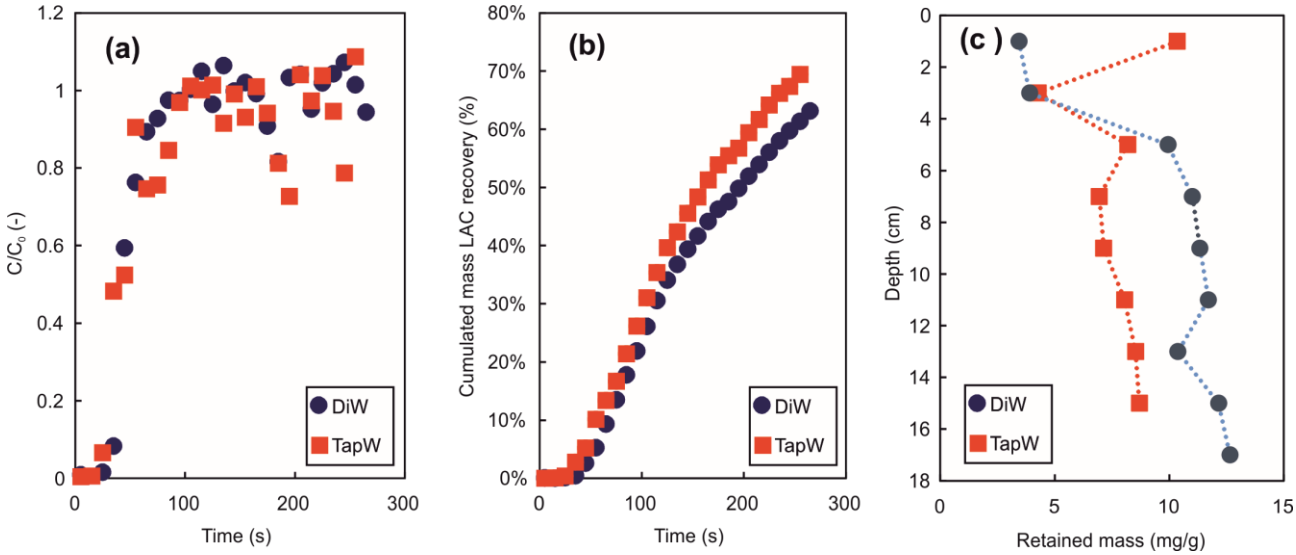

Figure 9. Column LAC transport tests: breakthrough curves (outflow concentration normalized to the concentration applied at column inlet, C_0 = 350 g/l) **(a)**, cumulated particle mass recovered at the column outlet (calculated as percentage with respect to the mass applied at column inlet) **(b)**, and profiles of retained particles at the end of the drainage tests (AC particle mass per unit mass of sand, mg/g) **(c).**

Tables

Table 1. Properties and characteristics of selected soils.

Parameter	Method	Value
Soil mineral		Silica sand (75-200 μm)
pH	ASTM D4972-13(1)	8.72
Bulk density (g cm^{-3})	ASTM D7263-09(2)	1.36
Porosity (%)	ASTM D4404-10(3)	32.5
Specific surface area (m^2 g^{-1})	EGME(4)	3.45
Organic matter (g kg^{-1})	UV-VIS(5)	3.55
Moisture content (%)	ASTM D2216-10(6)	0.0; 10.0
Dielectric constant (ε')	cavity perturbation(7)	6.98 (0%); 7.08 (10%)
Loss factor (ε'')	cavity perturbation(7)	0.68 (0%); 0.72 (10%)

(1) ASTM D4972-13. Standard Test Method for pH of Soils.

(2) ASTM D7263-09. Standard Test Methods for Laboratory Determination of Density (Unit Weight) of Soil Specimens.

(3) ASTM D4404-10. Standard Test Method for Determination of Pore Volume and Pore Volume Distribution of Soil and Rock by Mercury Intrusion Porosimetry.

(4) Simplified Ethylene Glycol Monoethyl Ether (EGME) procedure for assessment of soil surface area [11].

(5) UV-VIS Method - Test procedure for determining organic matter content in soils [11].

(6) ASTM D2216-10. Standard Test Methods for Laboratory Determination of Water (Moisture) Content of Soil and Rock by Mass

(7) Cavity perturbation method for dielectric properties measurements [11].

Table 2. Kinetic parameters and correlation coefficient (r^2) of the exponential kinetic model for all tests.

	Flu			**Ant**			**Pyr**			**Crh**		
P(W)	*k* (min^{-1})	*n*	r^2	*k* (min^{-1})	*n*	r^2	*k* (min^{-1})	*n*	r^2	*k* (min^{-1})	*n*	r^2
270 – 10 LAC	1.021	0.4684	0.968	1.325	0.3765	0.984	1.641	0.4471	0.999	1.956	0.5551	0.999
300 – 7.5 LAC	0.434	1.768	0.999	0.8494	0.7849	0.990	1.206	0.6811	0.999	1.654	0.6916	0.999
440 – 5 LAC	0.16	1.419	0.992	0.1356	2.005	0.997	0.7006	0.9001	0.996	1.363	0.8803	0.999
440 – 7.5 LAC	0.795	0.8396	0.999	-	-	0.987	1.094	0.9993	0.998	2.42	0.6282	0.999
440 – 10 LAC	0.926	0.8827	0.999	1.045	1.948	0.999	1.823	1.081	0.999	3.417	0.6277	0.999

Table 3. Column test parameters.

	Parameter	**Deionized water**	**Tap water**
Column properties	Sand mass (g)	60	60
	Column length (m)	0.182	0.180
Tracer test (saturated)	Total porosity (-)	0.48	0.46
	Hydrodynamic dispersion (m^2/s) ($x10^{-4}$)	9.45	8.06
	Pore volume (ml)	17.00	16.72
	Pore volume time (mins)	22.6	22.3
LAC drainage test (unsaturated)	Drained volume of LAC suspension (*) (%)	100	93.5
	Drained mass of LAC particles (*) (%)	63.1	69.4

(*) volume and mass balances at the end of the LAC drainage column test.

Supplementary Information

Table S1: Selected PAH-compounds from US-EPA list and their physical properties.

Compound	Molecular weight (g mol^{-1})	Boiling point (°C)	†Heat of vaporization (kJ mol^{-1})	‡log P	Chemical structure
Fluorene (Flu)	166	298	62.7	3.74	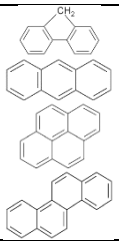
Anthracene (Ant)	178	340	52.4	3.95	
Pyrene (Pyr)	202	404	65.8	4.28	
Chrysene (Chr)	228	448	65.8	4.94	

‡ log P values calculated by ChemAxon

Table S2: Tap water composition.

Parameter	Value
pH	7.06
Total dissolved solid (mg/L)	584.2502
Hardness (°F)	36.60542
Electrical Conductivity (µS/cm)	676.16
Calcium (mg/L)	96.538
Magnesium (mg/L)	30.369
Chloride (mg/L)	39.713
Sulphate (mg/L)	93.953
Potassium (mg/L)	1.9712
Sodium (mg/L)	13.913
Bicarbonate (mg/L HCO_3)	276.372
Floride (mg/L)	0.072
Nitrates (mg/L NO_3^-)	31.349
Nitrites (mg/L NO_2^-)	0

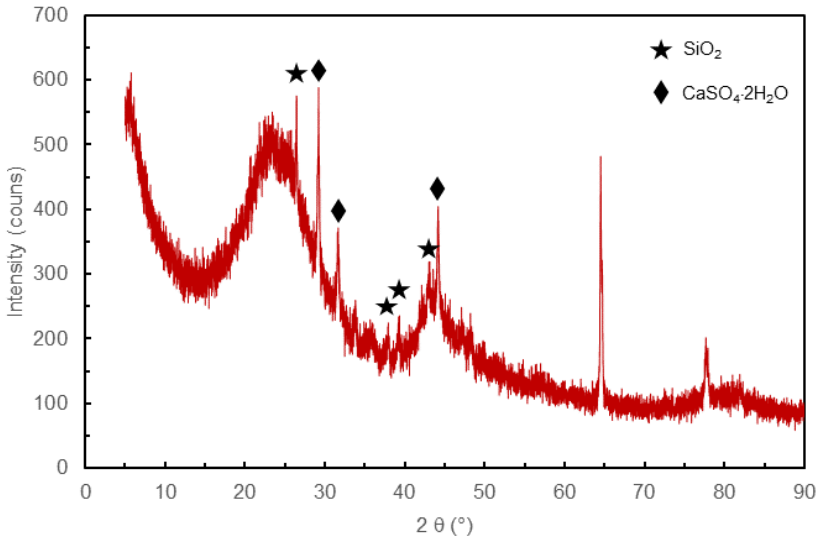

Figure S1: XRD pattern of stock LAC (particles dried at ambient conditions).

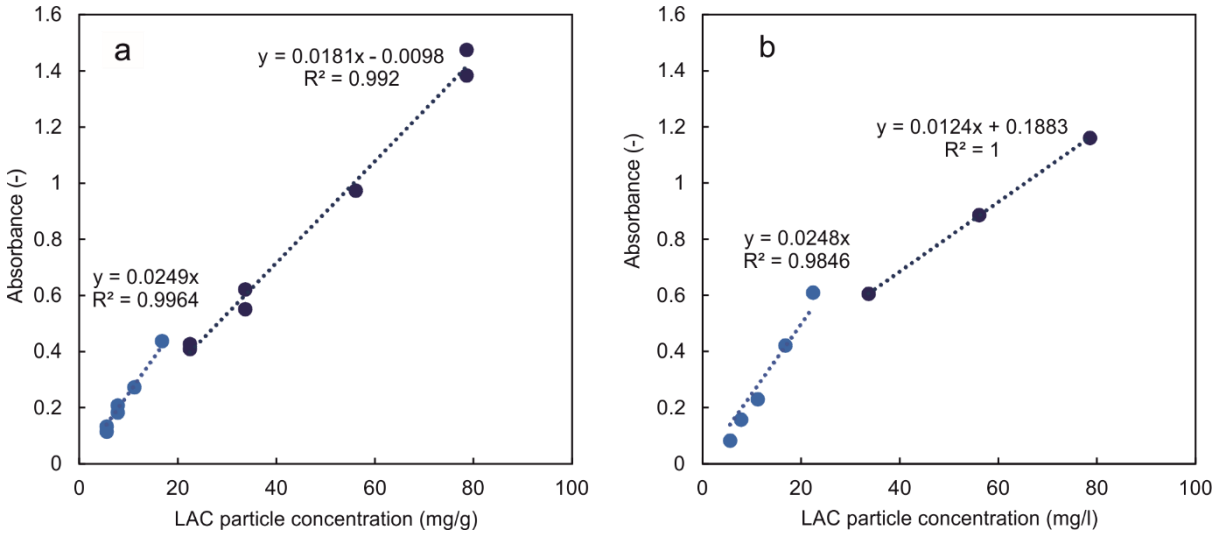

Figure S2: LAC calibration curves at λ=500 nm for particles dispersed in deionized water (a) and tap water (b). Both calibration curves evidenced a dual slope at all measured wavelengths. Thus, the two fitting curves were applied in the respective absorbance interval, and an average concentration was applied in the intermediate region.

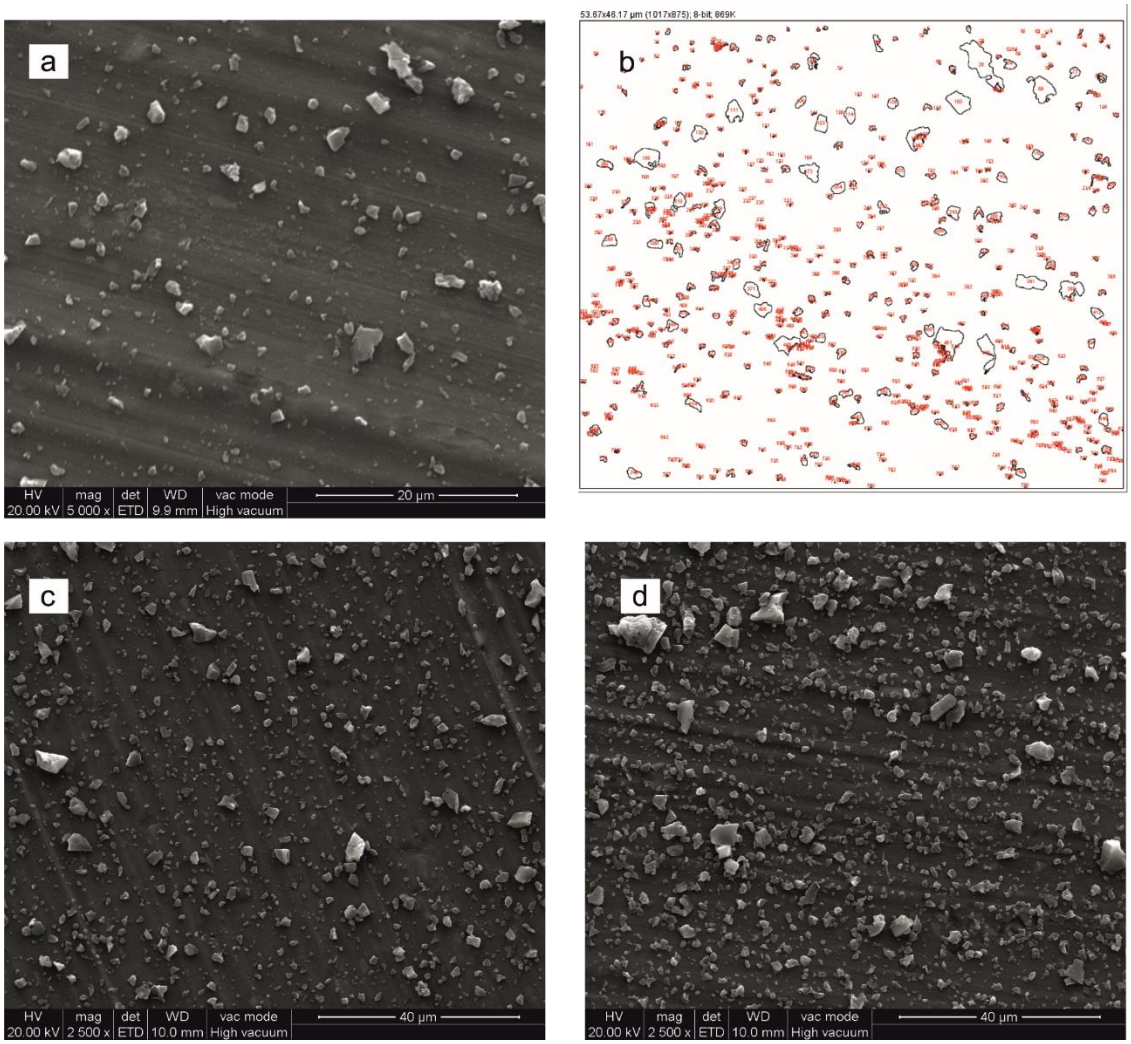

Figure S3: SEM images of LAC suspension diluted in deionized water. Sample 1 (particle concentration 16 mg/l): SEM image (a) and extracted particle areas obtained using the software ImageJ (b); SEM images of Sample 2 at 32 mg/l (c) and Sample 3 at 80 mg/l (d).

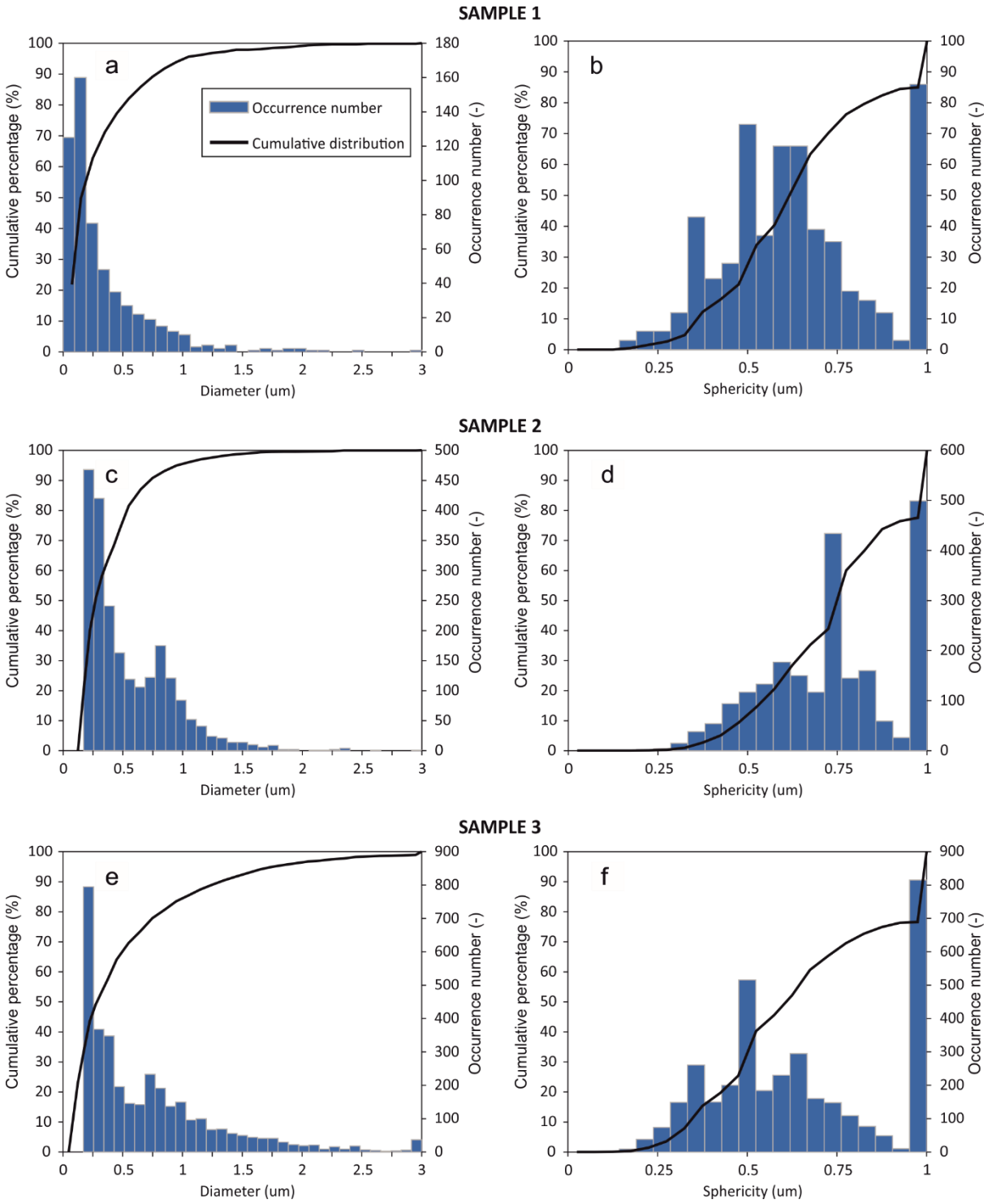

Figure S4: Sample 1: Size (a, c, e) and sphericity (b, d, f) distributions calculated using ImageJ from SEM images of Sample 1 (a, b), Sample 2 (c, d), and Sample 3 (e, f).

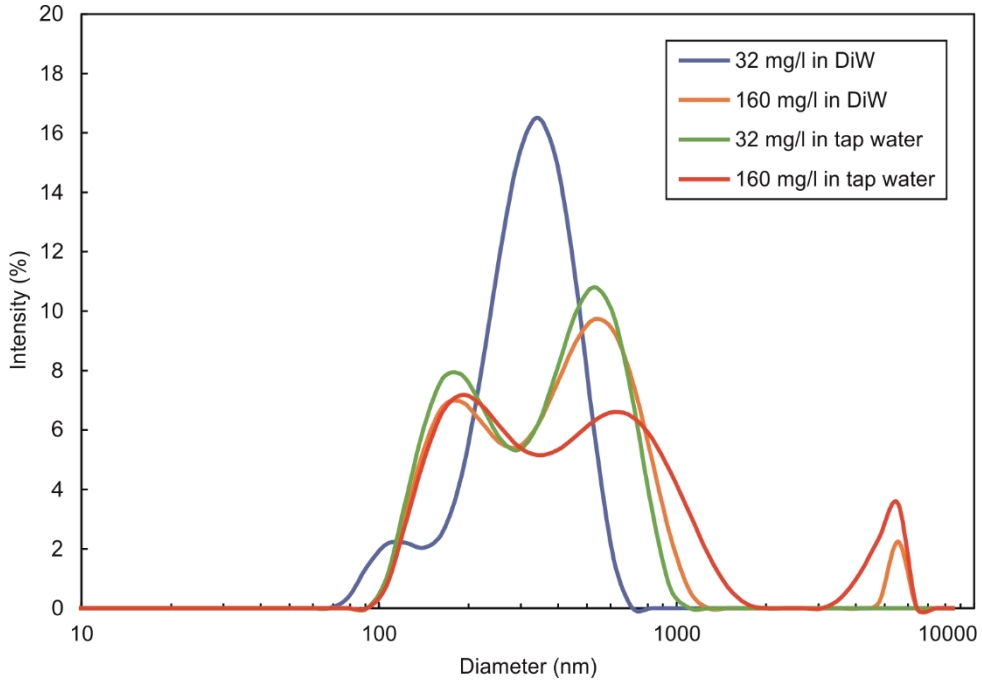

Figure S5: Intensity distribution of LAC at concentration of 100 mg/l and 500 mg/l in both DiW and tap water obtained with DLS analysis.

Table S 3: Single PAH-removal (%) for LAC-MW enhanced treatments.

#	t (min)	270 - LAC 10	300 - LAC 7.5	440 - LAC 5.0	440 - LAC 7.5	440 - LAC 10
Flu	0	0.00	0.00	0.00	0.00	0.00
	1	66.52	35.00	13.67	54.49	60.20
	2	0.00	77.60	38.37	77.14	81.84
	3	72.36	94.61	49.18	85.71	100.00
	5	96.71	98.27	80.61	-	-
Ant	0	0.00	0.00	0.00	0.00	0.00
	1	75.12	59.53	9.73	32.01	64.85
	2	-	70.71	44.78	75.14	98.23
	3	79.53	90.72	69.33	97.61	100.00
	5	97.22	96.02	96.29	-	-
Pyr	0	0.00	0.00	0.00	0.00	0.00
	1	80.93	70.28	52.10	67.00	83.85
	2	-	85.17	70.03	86.72	97.88
	3	91.38	91.76	84.63	98.78	100.00
	5	98.48	98.31	98.11	-	-
Crh	0	0.00	0.00	0.00	0.00	0.00
	1	85.88	80.44	74.21	91.15	96.71
	2	-	95.08	92.82	97.31	99.50
	3	97.11	94.93	96.02	99.65	100.00
	5	99.41	99.12	99.50	-	-

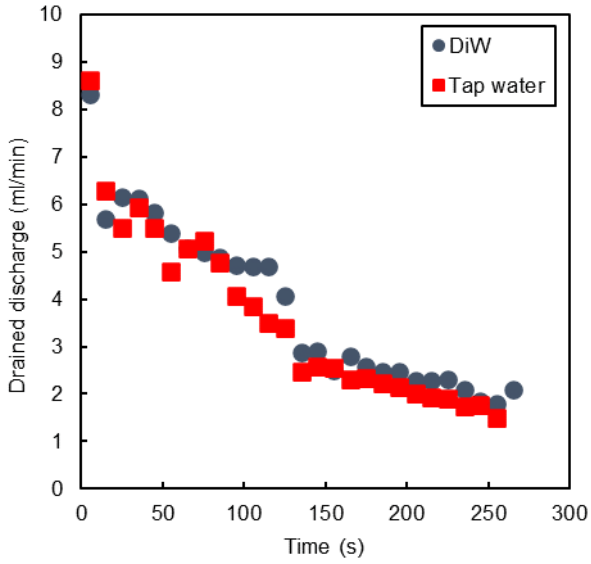

Figure S6: LAC drainage column tests: drained discharge reported as a function of time for LAC dispersed in deionized water and in tap water.